



Nanoscale

Patience is a Virtue: Self-Assembly and Physico-Chemical Properties of Cellulose Nanocrystal Allomorphs

Journal:	<i>Nanoscale</i>
Manuscript ID	NR-ART-06-2020-004491.R1
Article Type:	Paper
Date Submitted by the Author:	02-Aug-2020
Complete List of Authors:	Delepierre, Gwendoline; University of Fribourg Adolphe Merkle Institute, Polymer Chemistry and Materials Eyley, Samuel; KU Leuven, Chemical Engineering Thielemans, Wim; KU Leuven, Chemical Engineering Weder, Christoph; University of Fribourg Adolphe Merkle Institute, Polymer Chemistry and Materials Cranston, Emily; The University of British Columbia, Wood Science and Chemical and Biological Engineering Zoppe, Justin; Omya International AG

SCHOLARONE™
Manuscripts

ARTICLE

Patience is a Virtue: Self-Assembly and Physico-Chemical Properties of Cellulose Nanocrystal Allomorphs

Gwendoline Delepierre,^{a,c} Samuel Eyley,^b Wim Thielemans,^b Christoph Weder,^a Emily D. Cranston,^{c,*} and Justin O. Zoppe^{d*}

Received 00th January 20xx,
Accepted 00th January 20xx

DOI: 10.1039/x0xx00000x

Cellulose nanocrystals (CNCs) are bio-based rod-like nanoparticles with a quickly expanding market. Despite the fact that a variety of production routes and starting cellulose sources are employed, all industrially produced CNCs consist of cellulose I (CNC-I), the native crystalline allomorph of cellulose. Here a comparative study of the physico-chemical properties and liquid crystalline behavior of CNCs produced from cellulose II (CNC-II) and typical CNC-I is reported. CNC-I and CNC-II are isolated by sulfuric acid hydrolysis of cotton and mercerized cotton, respectively. The two allomorphs display similar surface charge densities and ζ -potentials and both have a right-handed twist, but CNC-II have a slightly smaller average length, aspect ratio and are less hygroscopic. Interestingly, the self-assembly behavior of CNC-I and CNC-II in water is different. Whilst CNC-I form a *chiral* nematic phase, CNC-II initially phase separate into an upper isotropic and a lower *nematic* liquid crystalline phase, before a slow reorganization into a large-pitch *chiral* nematic texture occurs. This is potentially caused by a combination of factors, including the inferred faster rotational diffusion of CNC-II and the different crystal structures of CNC-I and CNC-II, which are responsible for the presence and absence of a giant dipole moment, respectively.

Introduction

Chiral nematic liquid crystals (LCs) have become an integral part of our daily lives, due to their widespread use in the optoelectronics industry, especially in liquid crystal displays.¹ Recently, the chiral nematic LC forming ability of cellulose nanocrystals (CNCs) – needle-shaped colloidal cellulose nanoparticles – has attracted considerable interest.² Cellulose is a semi-crystalline biopolymer with a native crystal lattice (known as cellulose I) that can be transformed into several allomorphs through various chemical treatments.³ On the macroscale, such transformations induce a remarkable change of the twist angle of cellulose fibers, but their translation to the nanoscale structure and LC phases remains largely unexplored. In the various cellulose allomorphs, the cellulose macromolecules are arranged with different relative molecular orientations, leading to changes in inter- and intramolecular hydrogen bonding that extend either in the same plane or between different “sheets” of polymeric chains. The most widely studied allomorphs are cellulose I and II. Cellulose I is biosynthesized in higher plants, some microbes and a few animals in the form of semi-crystalline microfibrils, in which the polymer chains are organized in a parallel manner,

with their so-called reducing ends pointing all in the same direction.^{4,5} Cellulose II is obtained by either mercerization or regeneration of natural cellulose and is the most thermodynamically stable allomorph. It is commonly found in viscose or regenerated celluloses used in the textile industry.⁶ The mercerization process consists of treating cellulose with a concentrated sodium hydroxide solution that swells the cellulose bundles and disrupts hydrogen bonds, including those within the crystalline regions, resulting in a rearrangement of the polymer chains so that the direction of the reducing ends of neighbouring macromolecules with respect to the microfibril axis is anti-parallel. Nevertheless, the exact mechanism of this process is still unclear.⁷

To obtain highly crystalline CNCs, the less ordered regions in the cellulose supramolecular structure can be degraded, within a small window of conditions, using acids or oxidizing agents. The most commonly employed and well-studied process uses sulfuric acid hydrolysis with natural cellulose starting materials (often wood pulp and cotton) to produce nanocrystals in the cellulose I allomorph (CNC-I) in aqueous suspension.⁸ Concurrent with the cellulose hydrolysis reaction, an esterification also occurs that introduces some sulfate half-ester groups onto the surface of the nanocrystals, which imparts colloidal stability.⁸ The current interest in developing advanced materials with CNC-I is a result of their potential to be used as the basis for lightweight “green” nanomaterials with superior optical and mechanical properties and their ability to be produced industrially through relatively inexpensive and sustainable processes.⁹

In 1992, Revol *et al.* discovered that aqueous CNC suspensions can self-assemble into chiral nematic LC phases.¹⁰ To this day,

^a Adolphe Merkle Institute, University of Fribourg, Chemin des Verdiers 4, 1700 Fribourg, Switzerland.

^b Sustainable Materials Lab, Chemical Engineering, KU Leuven Kulak Kortrijk Campus, E. Sabbelaan 53 box 7659, 8500 Kortrijk, Belgium

^c University of British Columbia, 2424 Main Mall, Vancouver, BC V6T 1Z4, Canada.

^d Omya International AG, Baslerstrasse 42, 4665, Oftringen, Switzerland.

Electronic Supplementary Information (ESI) available: [details of any supplementary information available should be included here]. See DOI: 10.1039/x0xx00000x

this phenomenon is still intensely investigated and numerous patents have been filed (e.g., for security features in paper, optical filters and biocompatible pigments), although no commercial products based on CNC-I's unique optical properties exist to date.^{11,12} Above a critical concentration in water (c^*), CNC-I suspensions phase separate into an upper isotropic and a lower anisotropic (chiral nematic) phase. The volume fraction of the anisotropic phase increases linearly with increasing CNC-I concentration, passing through a biphasic regime prior to becoming a fully liquid crystalline suspension, where every pseudo (nematic) layer of nanocrystals is slightly rotated from one layer to the next, thus forming a helicoidal structure.¹³ The pitch is defined as the spacing between pseudo layers that are rotated by 360° and it dictates the wavelength of light that is reflected from the lyotropic LC phase.¹⁴ In aqueous suspensions, the pitch for CNC-I is on the micrometer scale; it is considerably reduced upon solvent evaporation, which leads to Bragg reflections in the visible region of the electromagnetic spectrum. Thus, CNC-I films produced by slowly drying chiral nematic suspensions act as photonic crystals. They reflect light at a wavelength whose maximum wavelength is given by the product of the pitch and the refractive index of the material and with the same handedness as the helix, which has been demonstrated to be always left-handed.¹³ Surprisingly, no studies have investigated the LC properties of CNCs of other allomorphs. Filling this void, we here report the first investigation of the LC properties of cellulose nanocrystals produced from cellulose II (CNC-II) and compare their assembly with that of typical CNC-I suspensions. To facilitate the comparison, the physico-chemical properties of CNC-I and CNC-II were extensively characterized and were found to be similar with the major difference being the crystalline allomorph. The mechanism that causes the helicoidal arrangement of CNC-I in LC suspensions is still under debate. One speculation is that it is caused by a right-handed twist in the nanocrystals themselves, and that this chirality is transferred into a left-handed helical assembly of the nano-rods.¹⁵ Indeed, high-resolution atomic force microscopy (AFM), transmission electron microscopy and cryo-scanning electron microscopy have provided images of individualized microfibrils or long CNC-I (isolated from tunicates and bacterial cellulose), in which a twist along the fibril axis can be observed.^{16–19} Ikkala and co-workers showed that the twist in an individual sulfated CNC-I nanocrystal is right-handed by electrostatically binding cationic gold nanoparticles to the negatively charged surface of the nanocrystals and determining their plasmonic response via circular dichroism (CD).²⁰ Additionally, Conley *et al.* determined the handedness of CNC-I via induced circular dichroism (ICD) by adsorbing the optically inactive dye Congo Red to the surface of the nanocrystals; a comparison of theoretical and experimental data also suggests that CNC-I have a right-handed twist.^{21,22} More recently, Ogawa analyzed the twist in long tunicate-derived CNC-I frozen in suspension via electron microdiffraction under cryogenic conditions and observed a continuous right-handed twist in the nanocrystals.²³ On the other hand, the twist of cellulose II has only been shown for macroscopic fibers and was simulated on the molecular level using chain sheet models,

suggesting a right-hand twist.³ However, there have been no studies on twisting or chirality of CNC-II.

Despite strong evidence for the nanocrystals themselves twisting, Schütz *et al.* reported that CNC-I suspensions begin to self-assemble into chiral nematic phases in water at spacings of ~ 51 nm,²⁴ and it is unclear if/how the nanocrystal twist could influence the interparticle interactions over such a long distance so that the chirality is translated to larger length scales. As such, electrostatic repulsive forces, which are relatively long range, may play a more decisive role and not (just) the twisted shape of the CNCs. This would imply the need for a chiral distribution of charges on the CNC surfaces, that force each layer to twist as the nematic layers approach one another.^{10,15,25} While discussed readily in the field, experimental evidence for the mechanism responsible for "chiral translation" in cellulosic materials remains elusive.

Recently, some attention has been given to investigating CNCs with different allomorphs, including cellulose II,^{26–32} and cellulose III.^{29,33,34} The focus of the work on CNC-II has been on the various preparation methods,^{26–28,32} with some discussion of properties^{29,32,34,35}, their enhanced enzymatic degradation,³⁶ and on their potential applications as bio-templates and dispersing agents.^{30,34} Three routes have been used to produce CNC-II, including (1) mercerizing CNC-I to CNC-II,^{26,29,37} (2) mercerizing macroscopic cellulose I to cellulose II, followed by an acid hydrolysis to produce CNC-II,³⁵ and (3) solubilizing cellulose during acid hydrolysis and subsequently recrystallizing, yielding CNC-II.^{28,32,34,38} Depending on the CNC-II production method, CNC-II have a lower aspect ratio and thus a more spherical particle shape when produced via route (1) and (2),^{26,28,30,32,34} and a more rod-like shape (higher aspect ratio) when produced via route (2).^{27,35} The CNC-II are typically shorter,^{27,29,34} even when less acidic conditions are used,²⁷ and many of the literature examples yield CNC-II with low surface charge that are not colloiddally stable due to the removal of sulfate groups when route (1) is used.^{26,37,39} To the best of our knowledge, the self-assembly of CNC-II have not yet been investigated. LCs with cellulose II (or cellulose II derivatives) are also entirely absent from the literature and the nanoscale chirality has not been shown experimentally for CNC-II.

In the light of these considerations, we report a detailed characterization of the morphological and colloidal properties of CNC-I and CNC-II, including an investigation of the twist via ICD. In addition, CNC-water interactions were elucidated using quartz crystal microbalance with dissipation monitoring (QCM-D), NMR and rheometry. The liquid crystalline features of CNC aqueous suspensions were determined by polarized optical microscopy (POM). Remarkably, the LC behavior of CNC-I and CNC-II suspensions is very different and a surprisingly slow assembly of CNC-II into chiral nematic phases having an unexpectedly large pitch was observed.

Results and discussion

Production of CNC-I and CNC-II

Cellulose II was accessed by first mercerizing cotton filter paper with 17.5% aqueous NaOH for 48 h, which yields complete allomorph conversion,^{26,40} and subsequently isolating CNCs by way of sulfuric acid hydrolysis (Fig. 1A). Wide-angle X-ray scattering (WAXS) showed the disappearance of the characteristic cellulose I peaks and the appearance of the cellulose II peaks after mercerization (Fig. 1B). This path was preferred over the mercerization of CNC-I to CNC-II, which gives colloiddally unstable CNCs, since our objective was to produce allomorphic CNCs with similar chemical properties, shape and dimensions, and it is known that *predictable* CNC LC properties require non-aggregated nanocrystals.

The acid hydrolysis protocol used to produce CNC-I and CNC-II was originally established for the isolation of CNC-I,⁴¹ using 64 wt% sulfuric acid, however, the hydrolysis time was shortened for cellulose II, to 25 min versus 35 min for cellulose I.^{27,29} This was based on work by Gong *et al.*, who reported that CNC-II hydrolyzed from cellulose II exhibited smaller dimensions and our goal was to obtain as similar nanocrystal lengths as possible. We chose to use the same concentration of acid to target similar surface charge densities for both allomorphs of CNCs. Our CNC-I and CNC-II were rod-shaped, sulfated and colloiddally stable, and WAXS experiments confirmed that no change occurred to the crystal structure during the acid hydrolysis process (Fig. 1B). More specifically, X-ray patterns for CNC-I exhibit a sharp peak at $2\theta = 22.3^\circ$ corresponding to the (2 0 0) plane with a shoulder at $2\theta = 20.2^\circ$ corresponding to the (1 0 2) plane. Two overlapping, weaker diffraction peaks are observed at $2\theta = 14.5^\circ$ and $2\theta = 16.4^\circ$, corresponding to the (1 $\bar{1}$ 0) and (1 1 0) planes, respectively. The peak at $2\theta = 34.0^\circ$ is assigned to the contribution of the (0 4 0) plane.⁴² For CNC-II, peaks at $2\theta = 12.4, 19.9,$ and 21.8° are assigned to the (1 $\bar{1}$ 0), (1 1 0), and (0 2 0) planes. Again, in both the mercerized cotton and CNC-II samples, the peaks that correspond to cellulose I are absent, supporting the successful allomorphic transformation and retention of the cellulose II crystal structure after acid hydrolysis.

Characterization of CNC-I and CNC-II

The chemical, physical and colloiddal properties of the two CNC types were comprehensively characterized (Table 1). The CNC shape and dimensions were investigated by AFM (Fig. 2). Both CNC-I and CNC-II appear as rod-like particles, as reported previously by Yue *et al.* and Gong *et al.*^{29,35} Even though a shorter hydrolysis time was used to produce CNC-II, these nanocrystals were slightly shorter and had a smaller height than CNC-I (after measuring >150 individual nanoparticles). For CNC-I, the average dimensions were a length of 140 ± 60 nm and a height of 7 ± 2 nm, yielding an aspect ratio of 20 ± 10 , while a length of 80 ± 20 nm, a height of 5 ± 1 nm, and an aspect ratio of 17 ± 6 , were determined for CNC-II. The CNC-II had a smaller particle size distribution than CNC-I, which may be attributed to partial depolymerization of cellulose chains caused by alkaline hydrolysis during mercerization (ESI, Fig. S2).^{43–45} In attempts to produce CNC-II with more similar dimensions to CNC-I, shorter hydrolysis times of 20 and 10 min were explored, but the effect

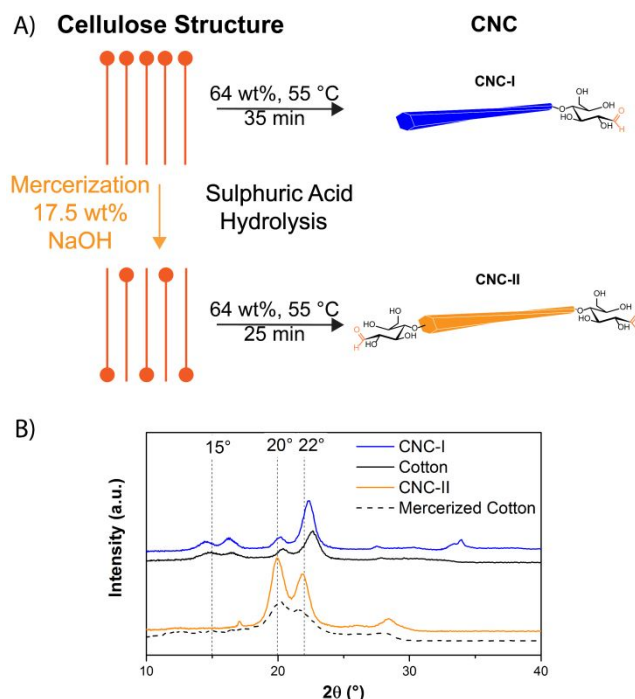


Fig. 1 (A) Schematic representation of the mercerization of cellulose I to cellulose II and the acid hydrolysis of the two cellulose allomorphs. In the mercerization process, the cellulose chains are rearranged into an anti-parallel configuration in which reducing-ends are found on both sides of the rod-shaped nanoparticles. Sulfuric acid hydrolysis of cellulose I and II affords the respective CNC-I (blue) and CNC-II (orange). Only one reducing end is shown at the end of a CNC for simplicity. (B) WAXS spectra of the two different CNC types and their starting materials, showing the successful conversion of cellulose I to cellulose II.

of this change on the nanocrystal size was minimal (ESI, Table S1).

The AFM images indicate that both allomorphs of CNCs tend to form lateral aggregates in clusters of 2-3 CNCs upon sample preparation, as also evident from the PeakForce™ error and overlay image shown in the ESI, Fig. S1. While the aggregation may be partly an artefact due to sample preparation/drying, this lateral aggregation has been reported previously by Elazzouzi-Hafraoui *et al.* for CNC-I in both dry and suspended samples.¹⁸ With respect to CNC-II, Sèbe *et al.* and Jin *et al.* reported lower aspect ratio CNCs, however their images were taken from CNC-II produced following path (1) described above, i.e., the mercerization was carried out on CNCs *after* hydrolysis.^{26,28} Dynamic light scattering (DLS) data support that the CNC-II prepared here are slightly smaller and there is minor aggregation in suspension giving an “apparent” size (spherical hydrodynamic diameter, D_h) of 110 nm and 84 nm for CNC-I and CNC-II,⁴⁶ respectively. Of note is that both allomorphs of CNCs disperse easily in water and form uniform colloiddal suspensions with a blueish hue.

We used SAXS as a complementary method to determine the cross-sectional dimensions of CNCs in suspension (ESI, Fig. S2). The form factor was fitted with an elliptical cylindrical model, consisting of a major and minor radius and cylinder length. The model resulted in a good fit to the data when a Schulz distribution was applied to the minor radius to represent the

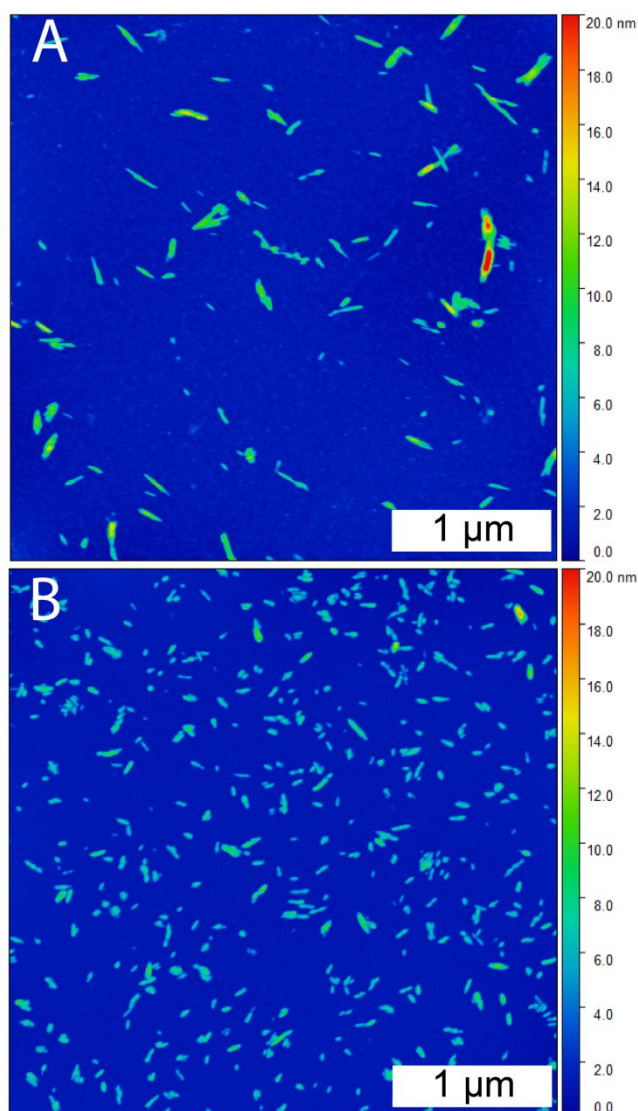


Fig. 2 AFM height images of (A) CNC-I and (B) CNC-II recorded in PeakForce™ mode for CNCs spin-coated on poly-L-lysine treated mica. The images show that all CNCs are rod-shaped with some lateral aggregation and the CNC-II are slightly shorter than CNC-I. (Scale bar = 1 μm)

particle size distribution (see Experimental Section and ESI, Fig. S3). CNC-I exhibited an average minor radius of 2.1 ± 0.2 nm, and an average major radius of 13 ± 2 nm. CNC-II were found to have a similar minor radius of 2.1 ± 0.1 nm and a major radius of 13.7 ± 0.9 . The length of the CNCs fell outside of the Q-range of the measurement, and therefore the length was fixed to that determined by AFM (*i.e.* 140 nm for CNC-I and 80 nm for CNC-II). The discrepancy in height between SAXS and AFM data is primarily due to tip convolution in AFM as well as drying artefacts.⁴⁷ In conclusion, both AFM and SAXS indicate similar cross-sectional dimensions for both allomorphs. Although the minor and major radii of CNC-I and CNC-II were similar, there was a significant difference in the breadth of their particle size distribution, with CNC-I presenting a much broader size distribution than CNC-II, similar to that measured by AFM (ESI, Fig. S4).

The average degree of polymerization (DP) of the cellulose chains comprising the two types of CNCs was determined following derivatization by carbanilation and subsequent gel permeation chromatography (GPC) analysis (ESI, Fig. S5).⁴⁸ The number- and weight-average molecular weights (M_n , M_w) and dispersity values (\mathcal{D}) are summarized in Table 1. While the M_n and M_w are of the same order of magnitude for both allomorphs of CNCs, the polymers making up CNC-I have a slightly higher dispersity than the chains forming CNC-II, with a \mathcal{D} of 6.77 vs. 5.85 for CNC-I and CNC-II, respectively. The lower cellulose dispersity may be correlated to the smaller particle size distribution seen by AFM and SAXS for CNC-II as well. The DP values for the two allomorphs of CNCs were calculated as 321 for CNC-I and 212 for CNC-II. The lower DP for the CNC-II indicates that some chain cleavage must have occurred during mercerization. Chain cleavage and imperfect mercerization may also lead to cellulose with more dislocated regions exhibiting more accessibility to acid hydrolysis, accounting for the slightly smaller dimensions measured by AFM (Fig. 2). Furthermore, the GPC shows a shoulder at low molecular weights for both allomorphs of CNCs, suggesting that the hydrolysis conditions employed were conducive to producing oligosaccharides, which then precipitated onto the CNC surfaces as described previously.^{41,49} The shoulders at low molecular weights for CNC-I and CNC-II are considered equivalent, which is expected given the similar starting materials and reaction conditions for the hydrolyses.

In support of the cellulose DP measurements, the concentration of available reducing end groups on CNC-I and CNC-II was determined using a bicinchoninic acid (BCA) colorimetric assay at pH 10.⁵⁰ Each cellulose chain should have one reducing end, but at pH 10 only a fraction of aldehydes are accessible due to the equilibrium between the cyclic hemiacetal group and the aldehyde. CNC-I had fewer reducing ends on a per weight basis (33 ± 2 $\mu\text{mol CHO/g CNC}$) than CNC-II (50 ± 2 $\mu\text{mol CHO/g CNC}$), which is in agreement with the smaller DP and the lower nanocrystal length observed for CNC-II. The anti-parallel arrangement of cellulose chains in CNC-II may also change the equilibrium and/or ability to detect aldehyde groups using the BCA assay. As there is a growing interest in reducing end modification of CNCs,^{50–53} the CNC-II allomorph might give higher yields and more successful end group modifications, which will be explored in future work.

The surface charge density of CNCs governs their colloidal stability which is an important factor in their self-assembly behavior.⁸ The surface charge densities for CNC-I and CNC-II were similar (Table 1 and ESI). Conductometric titrations^{54,55} (ESI, Fig. S6) were used to determine the overall surface charge per unit area⁵⁶ assuming cylindrical particles; charges of 0.52 e/nm^2 was determined for CNC-I and 0.51 e/nm^2 for CNC-II. This accounts for both sulfate half-ester groups and carboxylate groups on the CNC surface and these values are in the typical range for colloidally stable CNCs produced by sulfuric acid hydrolysis.⁴⁶ More specifically, CNC-I had 171 ± 3 $\mu\text{mol } -\text{OSO}_3^-/\text{g CNC}$ and 19 ± 2 $\mu\text{mol } -\text{COO}^-/\text{g CNC}$. CNC-II had a higher concentration of sulfate half-ester groups, 272 ± 1 $\mu\text{mol } -\text{OSO}_3^-/\text{g CNC}$, and nearly twice the concentration of

carboxylic acid groups, $42 \pm 3 \mu\text{mol} - \text{COO}^-/\text{g CNC}$. The higher concentration of carboxylate groups in CNC-II is likely due to random oxidation during the mercerization.⁵⁷ The difference in sulfate content is most likely due to the slightly smaller size of CNC-II, meaning they have a higher surface area and more accessible surfaces for esterification. Normalization by surface area is thus needed for a fair comparison ($0.464 -\text{OSO}_3^-/\text{nm}^2$ for CNC-I and 0.443 for CNC-II). Colloidal stability was also supported by ζ -potential measurements, which showed similar values for CNC-I and CNC-II (-35 ± 1 mV and -32 ± 1 mV, respectively) that correlate well with their surface charge densities.⁴⁶

Thermogravimetric analysis of neutralized CNCs was used to evaluate their thermal stability. Despite some differences in physical and chemical properties between the two allomorphs, their thermal degradation was almost identical, with the maximum weight loss at 299°C for CNC-I and 306°C for CNC-II (ESI, Fig. S7). In the case of sulfated CNCs, neutralization to the sodium salt form increases the thermal stability compared to the acid form CNCs,⁴⁸ and one of the authors of this work has recently shown that the surface charge density and cellulose DP are directly correlated to thermal stability.⁴⁸ Interestingly, despite the lower DP in CNC-II, they exhibit a slightly higher thermal stability, which is attributed to the higher thermodynamic stability of cellulose II.⁵⁸

CNC-I showed a higher shear viscosity than CNC-II in rheological measurements of 2 wt% aqueous suspensions, carried out with a cone and plate geometry (ESI, Fig. S10). The *trends* in viscosity with increasing shear rate were identical for both allomorphs of CNCs, but the viscosity was consistently lower for CNC-II. The measurements indicate a Newtonian plateau at low shear rates, a shear thinning region at intermediate shear rates, and another plateau at high shear rates, which is typical for isotropic CNC-I suspensions.⁵⁹ The lower viscosity of the CNC-II suspensions is likely a compound effect of the slightly smaller aspect ratio and a slightly higher surface charge density.^{55,60}

Table 1. Characterization of CNC-I and CNC-II.

Characterization	CNC-I	CNC-II
Length by AFM [nm]	140 ± 60	80 ± 20
Height by AFM [nm]	7 ± 2	5 ± 1
Aspect ratio from AFM	20 ± 10	17 ± 6
Equivalent spherical hydrodynamic diameter [D_h , nm]	110	84
Form factor (SAXS) minor radius [nm] ^{a)}	2.1 ± 0.2	2.1 ± 0.1
Form factor (SAXS) major radius [nm] ^{a)}	13 ± 2	13.7 ± 0.9
Number-average molecular weight, M_n [g/mol]	2.46×10^4	1.88×10^4
Weight-average molecular weight, M_w [g/mol]	1.67×10^5	1.10×10^5
Chain length dispersity (\mathcal{D})	6.77	5.85
Degree of polymerization	321	212
Reducing end groups [$\mu\text{mol CHO/g CNC}$]	33 ± 2	50 ± 2
Surface charge density [e/nm^2] ^{b)}	0.52	0.51
Sulfate half-ester groups [$\mu\text{mol} -\text{SO}_3^-/\text{g CNC}$]	171 ± 1	272 ± 1
Carboxylic acids [$\mu\text{mol} -\text{COO}^-/\text{g CNC}$]	19 ± 2	42 ± 3
ζ -potential [mV]	-35 ± 1	-32 ± 1
Maximum degradation temperature [$^\circ\text{C}$]	299	306
Normalized $\Gamma_{\text{H}_2\text{O}}$ [$\text{mg m}^{-2} \text{nm}^{-1}$] ^{c)}	1.6 ± 0.2	1.40 ± 0.03
Handedness of the nanocrystal twist	Right	Right
Excluded volume [m^3] ^{d)}	2.0×10^{-14}	1.2×10^{-14}

^{a)} Form factor determined by fitting an ellipsoidal cylinder model to SAXS curves with AFM length.

^{b)} Based on cylinder model with ellipsoidal section using the length from AFM and form factor from SAXS.⁵⁶

^{c)} The amount of water bound is normalized by the CNC film thickness.

^{d)} Calculated as described by Schütz *et al.*¹⁴

One apparent difference between CNC-I and CNC-II was that the neutralized, freeze-dried powders, showed a different re-dispersion behavior in water. Interestingly, the redispersion of CNC-II was effortless, in comparison to CNC-I, and at the same concentration, the CNC-II suspensions appeared less viscous. For CNC-I, probe sonication was required to reach the D_h measured for the never-dried material via DLS, whereas in the case of CNC-II simply shaking the vial by hand sufficed. This can be attributed to the formation of fewer inter-particle hydrogen bonds upon drying (due to the different crystal structure) and potentially from changes in the surface morphology of the CNCs.

To investigate water binding abilities of the two allomorphs, QCM-D measurements were performed on CNC films with a H₂O/D₂O solvent exchange procedure (ESI, Fig. S8).⁶¹ The amount of bound water ($\Gamma_{\text{H}_2\text{O}}$, in units of mg m⁻²), normalized by the CNC film thickness (in nm) was 1.6 ± 0.2 and 1.40 ± 0.03 mg m⁻² nm⁻¹ for CNC-I and CNC-II, respectively.⁶¹ While the difference is not statistically significant, the data suggest that CNC-II may have slightly less bound water on their surface. This is further supported by ¹H MAS NMR spectroscopic measurements, which show that in a controlled atmosphere with a relative humidity of $40 \pm 2\%$, a CNC-I film had an equilibrium moisture content of $13.5 \pm 0.2\%$ while this value was slightly lower for CNC-II ($11.7 \pm 0.1\%$), ESI, Fig. S9).^{62–66} Overall, this implies that CNC-II is slightly less hygroscopic than CNC-I, which is in agreement with experimental and computational studies on the wetting behavior of cellulose II,^{58,67} and CNC-II.⁶⁶

Twist in CNC-I and CNC-II

Direct imaging, e.g., via AFM or electron microscopy, of the axial twist of CNCs is challenging due to their small dimensions, especially for nanocrystals from higher plant sources, like the cotton starting material used here.^{16,17,68} One technique that has been used to infer the twist in CNCs is induced circular dichroism.⁶⁹ CD spectra of a CNC-I suspension spiked with Congo Red show a positive peak at the lowest energy transition (536 nm) and a smaller negative peak at 430 nm (Fig. 3), confirming a right-handed twist for our CNC-I. Since the CD response at lower wavelengths is strongly affected by the scattering of the reference CNC suspension (without dye), the wavelength range of 450–600 nm was considered for the determination of handedness (see ESI, Fig. S10). The CD spectrum of a Congo Red containing CNC-II suspension also shows a positive peak at 529 nm, i.e., at a similar position to CNC-I. Further, the higher energy states at 440 nm and 390 nm are more clearly resolved than for the CNC-I, as the signal is less obscured by scattering effects. The CD spectra thus suggest a right-handed twist for both CNC-I and CNC-II and the larger peak for CNC-II may indicate a higher twist frequency.²² This is in agreement with the simulations of Uto *et al.*, who used density functional theory optimization to show that cellulose II has a more twisted structure than cellulose I.⁷⁰

Self-assembly of CNC-I versus CNC-II

The self-assembly of CNC-I and CNC-II was studied in aqueous suspensions of increasing concentration (1 – 9 wt%) by observing their lyotropic LC behavior. The samples were made by diluting a 10 wt% stock suspension and experiments were carried out in 1 mM aqueous NaCl solution, where the salt was added to achieve a discrete double layer thickness of approximately 9.7 nm (i.e., relatively small but not fully screened surface charge).²⁵ The phase separation behavior was monitored in flat capillaries between crossed linear polarizers, initially over the course of six weeks (Fig. 4, top row). For CNC-I, the 1 wt% suspension remained isotropic, whereas at all other concentrations, phase separation into an upper isotropic and a

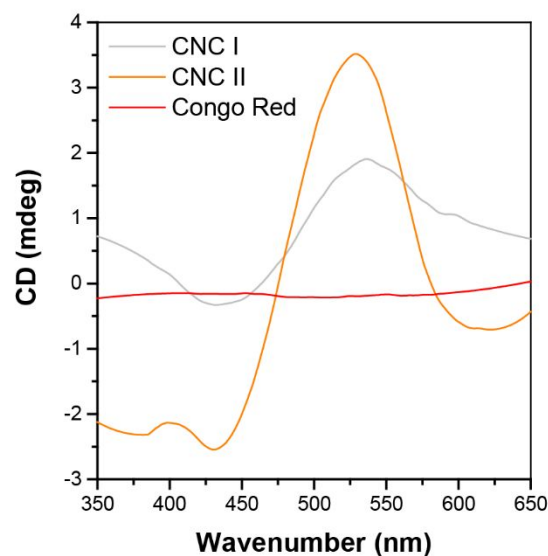


Fig. 3 ICD spectra of CNC-I (gray), CNC-II (orange) and Congo Red (red) showing a positive Cotton effect, implying a right-handed twist, for both allomorphs of CNCs.

lower birefringent phase occurred. The volume fraction of the chiral nematic phase increased with the CNC concentration as expected, but did not change significantly over time and equilibrated within 2 weeks.¹⁴ POM images show the fingerprint texture of a chiral nematic phase that is typical for CNC-I (Fig. 5A).¹⁰ The pitch was measured from POM images after 6 weeks, and decreased from 8.0 μm to 4.9 μm upon increasing the concentration from 4 to 9 wt%, which is comparable to literature values.¹²

In the case of CNC-II suspensions, birefringence was observed after 2 weeks only for concentrations above 5 wt% (Fig. 4, bottom row). Rather unexpectedly, the volume fraction of the birefringent phase decreased over time, until, for concentrations below 8 wt%, this phase disappeared. On the other hand, suspensions containing 8 and 9 wt% CNC-II still showed an anisotropic phase after 6 weeks. This result indicates that CNC-II have an increased critical concentration (c^*) for the onset of phase separation compared to CNC-I, which is consistent with their slightly lower aspect ratio,^{71,72} their doubled percolation threshold,⁸ and also highlights that the LC properties and textures formed in CNC-II suspensions are markedly distinct.

To confirm that CNC-II suspensions were indeed phase separating and not sedimenting, a large capillary was filled with a suspension with the highest CNC-II concentration tested (11.5 wt%, no added salt) in order to obtain a measurable amount of anisotropic phase that could be extracted using a micropipette (ESI, Fig. S12). The concentration of both phases was established gravimetrically after 6 weeks. The concentration of the upper phase was 10.957 ± 0.002 wt% while that of the lower phase was 12.169 ± 0.002 wt%, supporting that the CNC-II suspension phase separated. Note that a higher concentration in the anisotropic phase is also a feature of CNC-I phase separation, as Gray and co-workers reported values of ca. 1.5 wt% difference between upper and lower phases.^{73,74}

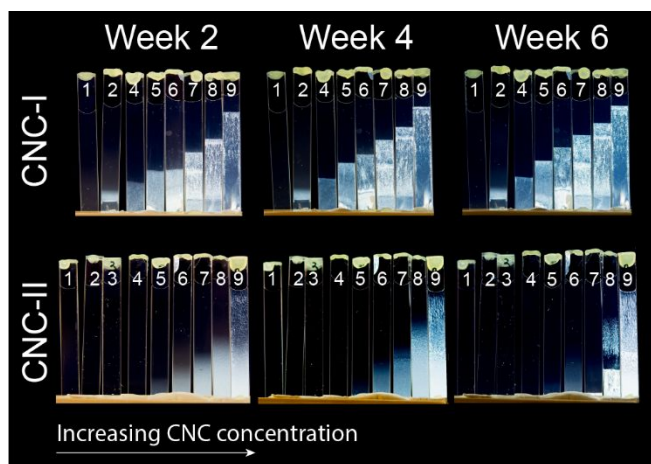


Fig. 4 Photos of aqueous CNC suspensions (with 1 mM NaCl) containing 1 – 9 wt% CNC-I or CNC-II taken between crossed linear polarizers. The pictures were taken at different time points (week 2, week 4, week 6) and illustrate the development of the LC phase separation over time (dark = isotropic phase, bright = birefringent/anisotropic phase; all capillaries are filled to a height of ca. 80%).

Furthermore, the lack of salt did not have a significant effect on the phase separation. Again, the surface charge density and ζ -potential of CNC-II imply good colloidal stability and sedimentation was not observed under any conditions.

Even at the highest CNC-II concentration shown in Figure 4, no chiral nematic structure was observed after 6 weeks (Figure 5B). Instead, a randomly oriented nematic phase formed, which is often referred to as a marble texture.⁷⁵ A nematic LC behavior was previously reported by Araki *et al.*, who observed nematic phases for high-aspect-ratio CNC-I derived from bacterial cellulose (in the absence of salt).²⁵ Although the CNC-II nanoparticles were found to be twisted according to the ICD experiment, not all twisted rod-shaped particles do exhibit chiral nematic phases. For example, some chiral filamentous bacteriophages have been reported to form nematic LCs, while others form chiral nematic LCs with little difference in building block chirality.⁷⁶ This was also observed previously by Dogic *et al.*; even though Pf1 and fd viruses have very similar structures, only the latter forms a chiral nematic phase.⁷⁷

Surprisingly, the formation of chiral nematic phases in CNC-II suspensions was “only” a matter of time, as became evident when the investigation was extended to 40 weeks. POM images of a 9 wt% CNC-II suspension taken after one and two weeks show that at first, a nematic phase forms, and at these time

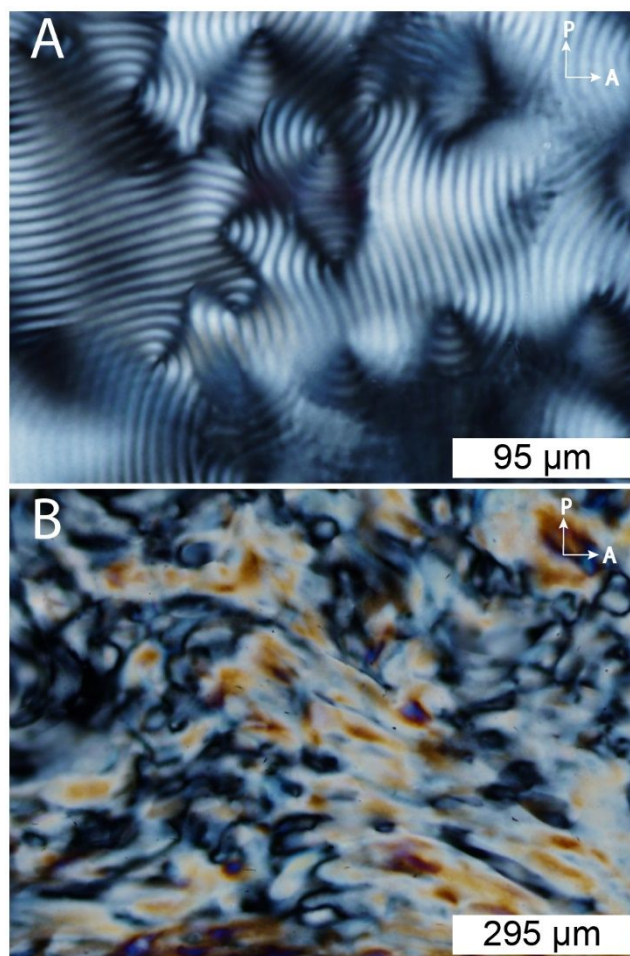


Fig. 5 POM images of aqueous CNC suspensions between crossed linear polarizers. (A) CNC-I suspension (5 wt% CNC-I, 1 mM NaCl, timepoint = 6 weeks), showing the characteristic fingerprint texture of the anisotropic phase. (B) CNC-II suspension (8 wt% CNC-II, 1 mM NaCl, timepoint = 6 weeks), showing a nematic marble texture.

points, nematic tactoids can be observed (Fig. 6A, B and ESI, Fig. S13). A retardation plate was added to show the orientation of the birefringence (blue – crystals oriented perpendicular to the slow light axis, or yellow – crystals oriented parallel to the slow light axis).⁷⁵ After 15 weeks, further thread-like textures were observed under POM, indicating that the liquid crystalline arrangement was still nematic, albeit with more orientation of the nematic axis normal to the plane of the flat capillary walls. Also, schlieren textures were observed in these samples, again characteristic of a nematic LC (Fig. 6C). The birefringent patches became more symmetric over time, with thinner thread-like structures, a more network-like pattern was formed, indicative of a long pitch chiral nematic phase (Fig. 6D).⁷⁸ Nevertheless, the line spacing (pitch) was not as well-defined in CNC-II suspensions, in comparison with the fingerprints formed in CNC-I suspensions. A much clearer chiral nematic texture for CNC-II suspensions was seen after 40 weeks (Fig. 7B), for which a pitch of $54 \mu\text{m}$ was measured. This dimension is about six times larger than the pitch observed for the same concentration CNC-I suspension after 40 weeks (i.e., $8.7 \mu\text{m}$).

Gray *et al.* reported a very similar nematic structure as observed here for CNC-II (Fig. 6) by subjecting a CNC-I suspension to shear.⁷⁵ The authors then followed the re-orientation of CNC-I

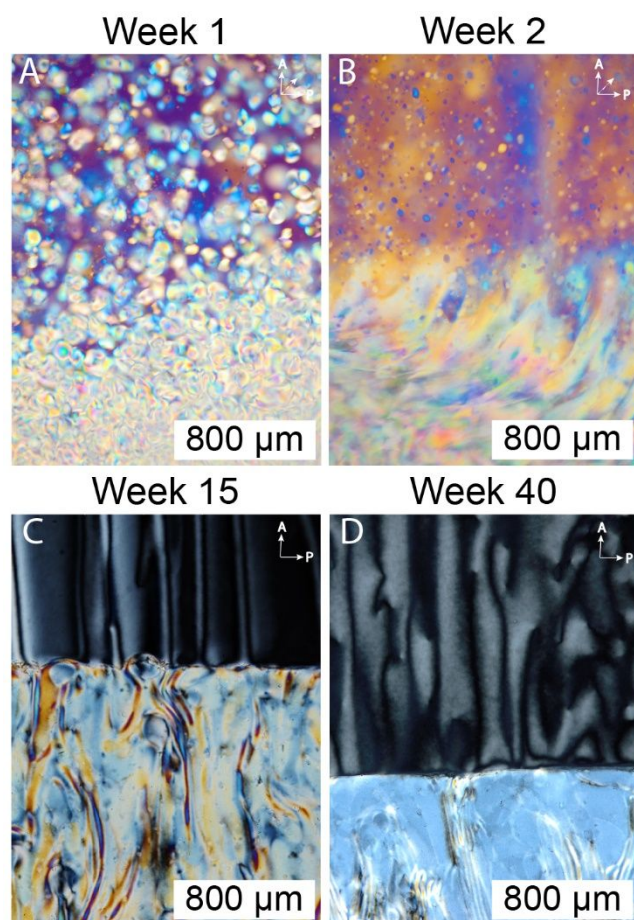


Fig. 6 POM images of an aqueous suspension containing 9 wt% CNC-II (with 1 mM NaCl), taken between crossed linear polarizers at different timepoints. (A) 1 week, (B) 2 weeks, (C) 3 weeks, and (D) 4 weeks. Images A and B were acquired with a retardation plate of 530 nm. (Scale bar = 800 μm)

over 24 h into a long pitch chiral nematic texture and attributed the transition to a twist-bend orientation.⁷⁵ It is possible that at longer times, the CNCs would have equilibrated into their typical chiral nematic phase. This twist-bend nematic reorientation has also been observed in CNC-I suspensions by Van Rie *et al.* using diffusion measurements,⁷⁹ and SAXS measurements further showed that CNC-I orient into nematic domains already within the macroscopically isotropic phase prior to phase separation occurring.⁸⁰ Our observations suggest that this reorientation is what happens for CNC-II, but on a much slower timescale.

The fact that CNC-II suspensions only exhibited detectable chiral nematic phases after such long periods, begs the question whether the morphology or surface chemistry of the nanocrystals had changed over time. In order to probe this, DLS, ζ -potential, and WAXS measurements were carried out after 12 months. The DLS data reveal that the size remained the same and no change was observed in ζ -potential (-31 ± 1 mV vs. -32 ± 1 mV), indicating that desulfation of CNC-II at room temperature was minimal.⁸¹ Furthermore, the WAXS spectrum of CNC-II still showed the characteristic peaks of cellulose II, confirming the stability of the crystalline structure (ESI, Fig. S14).

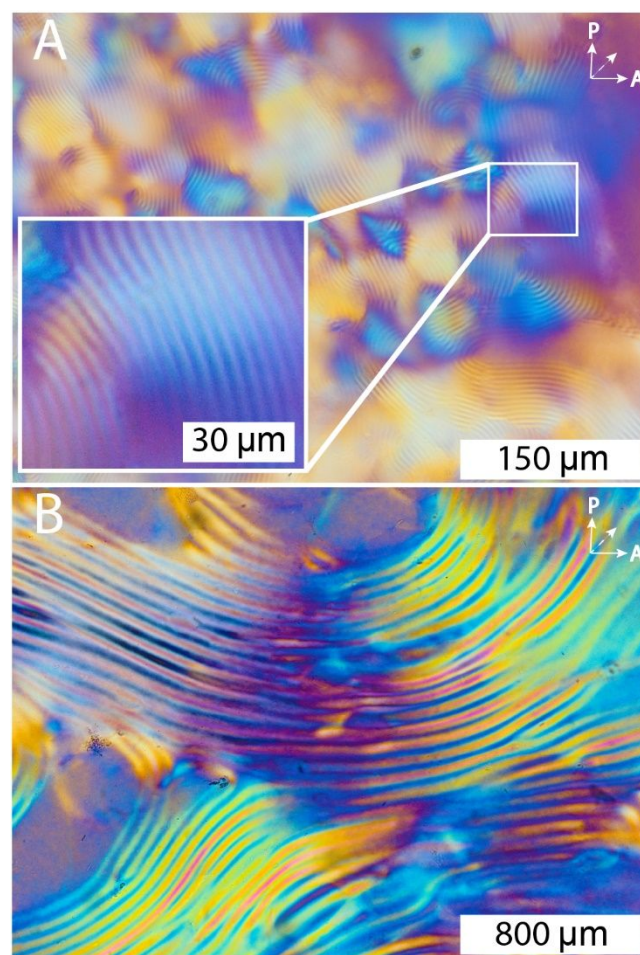


Fig. 7 POM images of CNC suspensions at 8 wt% (with 1 mM NaCl, 40 weeks) taken between crossed linear polarizers with a 530 nm retardation plate. (A) CNC-I suspension with a pitch of 8.7 μm and a zoomed in image showing the fingerprint texture in more detail and (B) CNC-II suspension showing a long chiral nematic pitch of 54 μm .

Based on these observations, we propose a few hypotheses to explain the CNC-II LC behavior. First, the CD measurements suggest a larger twist frequency in the individual CNC-II rods, which would result in a smaller displacement angle in between the nanocrystals when stacking, requiring more “layers” to make a full 360° turn and leading to a larger pitch; however, this does not explain the slow assembly.⁸² Alternatively, the different CNC-II self-assembly behavior could be the result of a different distribution of the sulfate half-ester groups on the surface of the nanocrystals (which appears to be exceedingly difficult to assess experimentally),⁸³ the different internal crystal structure, or the difference in the particle size.

The crystal structure may be another important factor responsible for the slow self-assembly of CNC-II due to the expected difference in permanent dipole moments for CNC-I and CNC-II. Frka-Petesic *et al.* quantified a giant dipole moment of 4400 ± 400 Debye along the CNC-I long axis.⁸⁴ This dipole is the result of the parallel orientation of the cellulose chains, and the high crystallinity in CNC-I. Strong dipole-dipole interactions between nanocrystals should induce alignment of CNC-I and this coupled with the cooperative effects that have been seen to kinetically enhance LC ordering⁸⁵ would dictate relatively fast self-assembly. In other LC systems, dipole moments have been

demonstrated to enhance the self-assembly behavior.^{86,87} On the other hand, CNC-II consist of cellulose chains in an anti-parallel structure, which would reduce or even nullify the permanent dipole moment of an individual nanocrystal, significantly reducing particle-particle interactions and, therefore, slowing their self-assembly.

Another potential explanation for the slower assembly of CNC-II lies in the slightly smaller particle length of CNC-II. The formation of the chiral nematic phase by CNC-I is entropically driven i.e., the loss in rotational degrees of freedom is outweighed by the increase in translational entropy upon CNC alignment.^{71,88} As a result of their shorter length, CNC-II have a smaller excluded volume ($1.2 \times 10^{-14} \text{ m}^3$ for CNC-II versus $2.0 \times 10^{-14} \text{ m}^3$ for CNC-I, Table 1), increasing their rotational entropy at the same concentration as CNC-I and shifting the rotation-translational diffusion thermodynamic interplay that leads to particle alignment to higher concentrations than for CNC-I.^{79,88} This increased rotational freedom for CNC-II could also be related to the longer time to reach the phase-separated equilibrium state. If the movement degrees of freedom and hence the diffusion coefficients (rotational and translational) of CNC-II are larger than for CNC-I, as we hypothesize based on their relative size, then the CNC-II require significantly higher concentrations to restrict rotational diffusion (i.e., higher c^*), potentially requiring more time to orient into a chiral nematic texture once adequately "confined" by the higher particle density.

While it would be ideal to compare CNCs with identical dimensions and size distributions, and which only differed in their crystalline allomorphs, it is very challenging to produce CNC-II with longer lengths or to produce smaller CNC-I by hydrolysis, as we reached the level-off degree of polymerization (LODP).⁸⁹ Therefore, we cannot draw conclusions as to which parameter has the greatest impact on the different self-assembly behavior of CNC-II compared to CNC-I. We encourage future work involving the self-assembly of CNC-II with larger aspect ratios, such as bacteria or tunicate-derived CNCs.

Conclusions

In conclusion, CNC-II were made from mercerized cotton and hydrolyzed with sulfuric acid to give nanocrystals with a slightly smaller aspect ratio, but similar surface charge density, as CNC-I. ICD indicated that both types of CNCs have a right-handed twist and QCM-D and ¹H MAS NMR spectroscopy suggest that CNC-II interact slightly less with water. Interestingly, the two allomorphs of CNCs show a very different LC behavior.

Concentrated CNC-II suspensions phase separated first into an isotropic and nematic phase, which eventually equilibrated into long pitch chiral nematic phases after an extended period of time, e.g. 40 weeks. In contrast, the equilibration of CNC-I into chiral nematic phases with a much smaller pitch took place in under two weeks. Because entropic phase transitions are a function of nanocrystal aspect ratio, and linked to their diffusion coefficients, the different assembly characteristics are partially attributed to the smaller average length of CNC-II. The twist frequency and dipole moment (or lack thereof in CNC-II) may

contribute to the slow onset of the chiral nematic phase in CNC-II suspensions but the magnitude of this contribution is unclear. Overall, our results show that changing the crystalline allomorph of CNCs can be used as a way to tune the chiral nematic pitch in both liquid crystal suspensions and dried CNC films, with potential as optical components/filters which now span a larger range of useful wavelengths (from visible into the far infrared). While the current commercial production of CNCs uses cellulose I as a starting source material, the same production process could be applied to cellulose II starting materials and furthermore, some current processes produce CNCs with a mixture of cellulose I and II allomorphs.⁹⁰ However, we are not proposing CNC-II production should replace CNC-I, merely that it is feasible if the differing properties were desirable in a particular application.

Future work exploring the acceleration of the self-assembly process would be beneficial, for example by exposing the CNC-II suspensions to external electromagnetic fields. Further experiments coupled with modelling, to understand the slow onset of chiral nematic textures for CNC-II suspensions, are needed. In any case, patience is a virtue when it comes to the self-assembly of CNC-II suspensions.

Experimental

Sulfuric acid (98%), Whatman n°1 cotton filter paper, sodium chloride, sodium hydroxide pellets, Congo Red, Dowex® Marathon™ C hydrogen form (SAC exchange resin) and dialysis tubing cellulose membrane (MWCO 14 kDa) were all purchased from Sigma-Aldrich. Congo Red was purified by Soxhlet extraction with 87.5% 2-propanol/12.5% distilled water (DI) for 6 h. All other chemicals were used without further purification. Millipore-processed deionized water (milli-Q) was used with a resistivity of 18.2 mΩ cm.

Mercerization of cotton filter paper

Whatman n°1 cotton filter paper (30 g) was cut into pieces of ca. 2 x 2 cm that were mercerized in 17.5 wt% NaOH solution (1 kg) at room temperature. The mixture was stirred for 24 h on an IKAKS 260 basic magnetic stirrer. The mercerized cotton filter paper was filtered off with a Büchner funnel (without filter), to remove the NaOH solution, and was further washed with water until the pH of the wash water was neutral. The mercerized paper was then dried at 40 °C in a vacuum oven overnight.

Isolation of CNC-I: Cellulose nanocrystals were made by the hydrolysis of Whatman n°1 cotton filter paper (30 g) with sulfuric acid (64 %, 420 mL) at 55 °C using a previously published protocol.⁴¹ The filter paper was cut into small pieces of ca. 1 x 1 cm, and added to the stirred acid over the course of 5 min. After the addition was complete, the mixture was stirred with a mechanical stirring rod for 30 more min. The reaction was quenched by two-fold dilution with ice-cold DI water (840 mL), followed by three subsequent centrifugation and redispersion steps of the obtained pellet in DI water (20,000 g, 30 min) until the CNC-I no longer sedimented. The CNC-I were transferred to pre-washed dialysis tubes (MWCO = 14 kDa) and dialyzed

against milli-Q water until the pH of the suspension and the conductivity of the dialysis water were constant. The final suspension was tip-sonicated using a Branson Sonifier SFX550 for 5 min at 10% amplitude before it was filtered through a fritted glass filter with porosity 4. A yield of 55% was determined gravimetrically and the CNC-I suspension was stored at 2 wt% in acid-form in a refrigerator. A small portion of the CNC-I were freeze-dried on a Telstar LyoQuest lyophilizer in sodium form (a dilute NaOH solution was added until neutral pH was obtained) for further analysis.

Isolation of CNC-II

The same procedure as for CNC-I was followed for CNC-II, but mercerized cotton filter paper was used and the hydrolysis time was decreased to a total of 25, 20 or 10 min including the addition time of cellulose II to the acid. A yield of 26% was obtained for CNC-II and the suspension was stored at 2 wt% in acid-form in a refrigerator. A portion of the CNC-II were freeze-dried in their sodium form, following the same procedure as for CNC-I.

Wide angle X-ray scattering

CNC-I and a CNC-II suspensions (1 mL, 2 wt%) were added into a small glass vial with a diameter of 0.5 cm, the suspensions were left to dry in ambient conditions in order to form a film. The film was removed from the vial and attached to a holder. The WAXS spectra was recorded with NanoMax-IQ camera (Rigaku Innovative Technologies, Auburn Hills, MI, USA). The camera was equipped with a Cu target sealed tube source (MicroMax 003 microfocus Rigaku) and the scattering data were recorded by a Pilatus100 K detector (Dectris). The CNC film was kept under vacuum at room temperature during the measurement. Raw data were processed with Mathematica.

Atomic force microscopy (AFM)

Freshly cleaved mica was functionalized with an aqueous poly-L-lysine solution (0.1 %) by drop-casting 40 μ L onto mica, waiting for 30 s, washing the substrate with milli-Q water, and drying under a nitrogen flow. CNC suspensions (0.001 wt%, 30 μ L) were spin-coated, with a Laurell WS-650-23 B spin coater, onto the functionalized mica at 2000 rpm and subsequently washed with milli-Q water and dried under a nitrogen flow. AFM images were acquired on a Multimode AFM Nanoscope-VIII from Bruker (Santa Barbara, CA, U.S.A.) using PeakForce™ ScanAssyst mode, at room temperature, with NCHR-20 probes from NanoWorld with a nominal spring constant of 42 N/m. The length and height of the CNCs was measured with Gwyddion on approximately 150 non-touching rod-shaped particles and the data was processed using Origin software. The AFM images shown were adapted using Gwyddion, the images were levelled by applying a mean plane subtraction and the horizontal pixel jumps were removed.

Small angle X-ray scattering (SAXS)

Small angle X-ray scattering measurements were performed on a Xenocs Xeuss 2.0C laboratory beamline equipped with an ultra-low dispersion copper K α X-ray source and DECTRIS Eiger 1M detector. The X-ray beam was collimated to 0.5 mm diameter at the sample, with samples (CNC-I and CNC-II suspensions of 1 to 10 wt%, containing 1 mM added NaCl) loaded into 0.9 mm diameter borosilicate glass capillaries. The entire beam path was evacuated to <10 mbar prior to measurements to reduce parasitic scattering contributions. Sample to detector distance was calibrated by measurement of silver(I) behenate prior to sample data acquisition.

2D to 1D data reduction was performed using Foxtrot (Xenocs/Synchrotron du Soleil) with absolute intensity scaling according to the transmitted beam intensity measured prior to an post data collection. Subtraction of a 1 mM sodium chloride blank was performed prior to further data analysis.

1D data fitting was performed using Sasview (version 4.2.0) using the inbuilt elliptical cylinder model. The length of the cylinder was fixed to the length provided by AFM to prevent interference of the length parameter in the data fitting as it was outside the Q range of the data. Minor radius and an axis ratio (minor:major radius), along with particle size distribution of the minor radius (Schulz distribution) were fitted to the data. The scattering length density of cellulose was fixed to 14.7 \AA^{-2} .

Determination of CNC degree of polymerization (DP)

The DP was measured following a modified derivatization procedure of Vanderfleet *et al.*⁴⁸ Freeze-dried CNCs in sodium form were placed in an oven at 80 °C for 1 h to remove residual moisture. Then, 25 mg of CNC-I or CNC-II were placed in a glass vial, 10 mL DMSO and 1 mL phenyl isocyanate were added. The reaction was performed at 70 °C for 40 h in closed vials whilst stirring. The reaction was quenched by adding 2 mL of methanol to the vial. Gel permeation chromatography (GPC) measurements of the carbanilated CNCs was performed on an Agilent 1100 with DMSO that contained 0.5% LiBr as eluting solvent. Carbanilated CNCs were injected at a concentration of 0.25 g/mL at an eluting rate of 0.5 mL/min. Polystyrene sulfonate with molecular weights of 891, 2000, 4290, 10000, 29500 and 140000 Da were used as calibration standards. The quantification of cellulose tricarbanilates was performed with a Waters 486 UV spectrophotometer at 254 nm. The DP of cellulose was calculated by dividing the weight-average molecular weight by the molecular weight of tricarbanilated anhydroglucose unit (519 g/mol).

Reducing end-group quantification

Bicinchoninic acid assay (BCA) was used to quantify the number of reducing end-groups on the CNCs as previously reported by Risteen *et al.*⁵⁰ Step 1: two solutions were prepared: Solution A (pH 9.7), contained Na₂CO₃ (5.428 g), NaHCO₃ (2.42 g), and BCA disodium salt hydrate (0.1942 g) in milli-Q water (100 mL). Solution B contained CuSO₄·5 H₂O (0.1248 g) and L-serine (0.1262 g) in milli-Q water (100 mL). Step 2: a calibration curve was prepared with a 0 – 80 $\times 10^{-6}$ M glucose solution. For each concentration in the calibration curve, 2 mL of glucose solution,

1 mL of solution A and 1 mL of solution B were added to a glass vial with a cap and stirring bar. Step 3: to glass vials, CNC-I or CNC-II (5.0×10^{-3} g) were added together with 1 mL of solution A and B. All the vials (CNC suspensions and glucose solutions) were heated to 75 °C for 30 min in a water bath. The vials were then cooled to room temperature, the CNC samples were centrifuged at 5000 rpm to remove the CNCs, and the absorbance of the glucose solutions and the supernatants of the CNC samples were measured at 560 nm. The experiments were done in triplicate.

Conductometric titrations

Conductometric titration were performed with a SevenCompact Duo pH/conductivity probe (Mettler Toledo) following the procedure by Beck *et al.*⁵⁴ Prior to conductometric titration, the suspensions were passed through a strong acid cation exchange resin column (12 g SAC/1 g CNCs). A 10 mM NaOH suspension was prepared, its concentration was standardized with the primary standard potassium hydrogen phthalate (KHP) by using phenolphthalein as an indicator. Then, 20 mL of a 0.796 wt% CNC suspension containing 1 mM NaCl was titrated against 10 mM NaOH solution. The first equivalence point indicates the number of sulfate half ester groups, the difference between the first and the second equivalence point indicates the number of carboxylic acid groups.

ζ-potential and dynamic light scattering (DLS)

A suspension of 0.25 wt% CNCs containing 5 mM NaCl was prepared to measure the ζ-potential. Prior to measurement, the suspension was bath sonicated for 10 min in ice-cold water. The measurements were recorded on a Malvern Panalytical Zetasizer Nano-ZS. An average of 10 measures were taken. The ζ-potential suspension was diluted 10 times for the DLS "apparent size" measurements, re-sonicated and measured on the same instrument.

Thermogravimetric analysis

Thermogravimetric analyses (TGA) were performed on a Pyris 6 thermogravimetric analyzer (PerkinElmer), with a sensitivity of 0.2 μg, at a heating rate of 10 °C/min, between 50 °C and 500 °C. The TGA was purged with a sample purge flow rate of 20 mL/min and a balance flow rate of 20 mL/min. Freeze-dried CNCs in sodium form (5 to 10 mg) were pressed into a pellet prior to measurement by compressing the freeze-dried powder in a 1 mL syringe with a rubber plunging head forming a pellet with a height of ca. 1 mm. The curves were smoothed in Origin using the Savitzky-Golay method.

Quartz crystal microbalance with dissipation (QCM-D)

CNC films were prepared by spin-coating a 1 wt% CNC suspension onto QCM-D silica-coated Au sensors at 3000 rpm for 60 s. The CNCs were annealed to the sensor surface by placing the samples in an oven at 80 °C for 15 min. Film thickness was determined using a UV-Vis (350 nm – 1800 nm)

spectroscopic ellipsometer from J.A. Woollam, M2000, with an incident angle of 72°. Thicknesses were modelled using a classic Cauchy model of two separate layers consisting of an SiO₂ layer (coating on the QCM sensor) and the CNC film. The sensors were placed in the QCM-D flow cell and equilibrated overnight at a rate of 0.2 mL/min, at RT in order to obtain a stable baseline. The changes in resonance frequency (Δf) and dissipation energy (ΔD) upon exchanging water for D₂O were measured using a Biolin Scientific QCM-D. After 30 min, D₂O was exchanged back to water. The amount of bound surface water ($\Gamma_{\text{H}_2\text{O}}$) was calculated according to the Sauerbrey equation:

$$\Gamma_{\text{H}_2\text{O}} = -C \left(\frac{\Delta f}{n} \right)_{\text{film H}_2\text{O}} \quad (1)$$

Where $\Delta f = f - f_0$ is the resonance frequency, n the measurement overtone number, and C is the sensitivity constant of the sensor.^{61,91,92} The $\Gamma_{\text{H}_2\text{O}}$ was normalized to the thickness of the CNC films.

Circular dichroism (CD) measurements

CNC-I and CNC-II were neutralized by adding NaOH. 3 mL vials containing 1.85 wt% suspensions of CNCs were prepared by diluting a more concentrated neutralized CNC suspension with milli-Q water. Either a stock solution of Congo Red (18.5×10^{-4} M, 0.03 mL) or an equal volume of milli-Q water was added to the suspension in order to reach a final concentration of CNCs (3 mL) of 1.85 wt% and a final concentration of 18.5 μM of Congo Red. Congo Red was left to adsorb overnight and the suspensions were shaken before measurements. The spectra were recorded on a Jasco Spectropolarimeter at 25 °C in a 1 cm pathlength cuvette with a scanning speed of 50 nm/min, and a bandwidth of 2 nm. The curves shown are the results from three subsequent measurements that were averaged and further smoothed with the Savitzky-Golay method in Origin.

Magic-angle spinning nuclear magnetic resonance (¹H MAS NMR) spectroscopy

The NMR experiments were performed on a Varian Unity Inova 400 spectrometer, using a Varian/Chemagnetics 3-channel 4 mm T-3 MAS probe. Radio frequency field strength was 80 kHz for ¹H decoupling. All experiments used a spinning rate of 5 kHz. Water was used as references for ¹H NMR experiments. The spectra were deconvoluted using a voigt-profile in Matlab. **Rheology:** Aqueous suspensions of CNC-I and CNC-II at 2 wt% were analyzed using a Kinexus Ultra+ rotational rheometer. The rheometry was performed under controlled shear rate mode, using a 4°/40 mm cone and plate measuring system. Steady state viscometry was performed in the shear rate range of 0.01–100 s⁻¹.

LC phase separation experiments

The CNC suspensions (100 mL, 2 wt%) were concentrated to 10 wt% by blowing N₂ over the suspensions whilst stirring. The concentration was determined gravimetrically. The 10 wt% stock suspension was then diluted from 1 to 9 wt% in small vials

and 10 μL of a 30 mM NaCl solution was added in order to make suspensions containing 1 mM of NaCl, so that the vials contained 0.3 mL CNC suspension. Prior to filling the capillaries, the suspensions were bath sonicated for 30 min with cooling. Capillaries (0.3 mm x 6 mm x 45 mm) were filled with the suspensions and put in a holder, the capillaries were sealed by either black nail polish or with an epoxy resin. The capillaries were photographed in between crossed linear polarizers, with white light shining from the back. Their percentage of anisotropic phase was measured using the Fiji software, Fiji is an image processing package for ImageJ software (National Institutes of Health),⁹³ by dividing the measured anisotropic phase by the total amount of suspension in the capillary.

Polarized optical microscopy

Images were acquired in reflection mode on an Olympus BX41 microscope equipped with a digital camera and for some images a 530 nm retardation plate was added. Polarized optical microscopy images were collected with crossed linear polarizers, which were oriented horizontally and vertically relative to the analyzer and, if used, the 530 nm wave plate was aligned from the bottom right direction to top left of the images. The pitch was measured using the Fiji software,⁹³ the measurement was taken over more than 20 half-pitches on 3 different locations.

Conflicts of interest

There are no conflicts to declare.

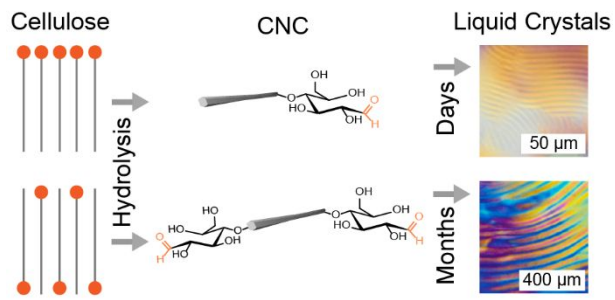
Acknowledgements

GD thanks Oriana Vanderfleet for performing a carbanilation reaction on the CNCs and for conducting the GPC measurements, Dr. Elina Niinivaara for her help with QCM-D, Behzad Zakani for his help with rheology measurements, and Francesco D'Acierno for performing the NMR measurements. Professors Scott Renneckar, Feng Jiang, Mark MacLachlan and Dana Grecov are acknowledged for access to equipment, training and lab facilities at the University of British Columbia. GD is grateful for the interesting discussions surrounding the data presented herein with Prof. Derek Gray (McGill University). GD and JZ acknowledge funding provided by the Swiss National Science Foundation (SNSF) (Ambizione Grant No. PZ00P2_167900) and GD, CW, and JZ thank the Adolphe Merkle Foundation for support. SE and WT acknowledge financial support from KU Leuven (C14/18/061 and IDN/19/014) and Research Foundation Flanders (G.0C60.13N) as well as the European Union's European Fund for Regional Development, Flanders Innovation & Entrepreneurship, and the Province West-Vlaanderen (Accelerate3 project, Interreg Vlaanderen-Nederland program). This work benefited from the use of the SasView application, originally developed under NSF award DMR-0520547. SasView contains code developed with funding from the European Union's Horizon 2020 research and innovation program under the SINE2020 project, grant agreement No 654000.

Notes and references

- J. P. F. Lagerwall and G. Scalia, *Current Applied Physics*, 2012, **12**, 1387–1412.
- E. Kontturi, P. Laaksonen, M. B. Linder, Nonappa, A. H. Gröschel, O. J. Rojas and O. Ikkala, *Advanced Materials*, 2018, **30**, 1703779.
- K. Kafle, K. Greeson, C. Lee and S. H. Kim, *Textile Research Journal*, 2014, **84**, 1692–1699.
- K. Hieta, S. Kuga and M. Usuda, *Biopolymers*, 1984, **23**, 1807–1810.
- R. H. Atalla and D. L. Vanderhart, *Science*, 1984, **223**, 283–285.
- F. J. Kolpak, M. Weih and J. Blackwell, 9.
- C. Yamane, H. Miyamoto, D. Hayakawa and K. Ueda, *Carbohydrate Research*, 2013, **379**, 30–37.
- Y. Habibi, L. A. Lucia and O. J. Rojas, *Chem. Rev.*, 2010, **110**, 3479–3500.
- D. Klemm, E. D. Cranston, D. Fischer, M. Gama, S. A. Kedzior, D. Kralisch, F. Kramer, T. Kondo, T. Lindström, S. Nietzsche, K. Petzold-Welcke and F. Rauchfuß, *Materials Today*, 2018, **21**, 720–748.
- J.-F. Revol, H. Bradford, J. Giasson, R. H. Marchessault and D. G. Gray, *International Journal of Biological Macromolecules*, 1992, **14**, 170–172.
- B. Frka-Petesic and S. Vignolini, *Nat. Photonics*, 2019, **13**, 365–367.
- R. M. Parker, G. Guidetti, C. A. Williams, T. Zhao, A. Narkevicius, S. Vignolini and B. Frka-Petesic, *Adv. Mater.*, 2017, **13**.
- J. P. F. Lagerwall, C. Schütz, M. Salajkova, J. Noh, J. Hyun Park, G. Scalia and L. Bergström, *NPG Asia Mater*, 2014, **6**, e80–e80.
- C. Schütz, J. R. Bruckner, C. Honorato-Rios, Z. Tosheva, M. Anyfantakis and J. P. F. Lagerwall, *Crystals*, 2020, **10**, 199.
- M. Khandelwal and A. Windle, *Carbohydrate Polymers*, 2014, **106**, 128–131.
- G. Nyström, M. Arcari, J. Adamcik, I. Usov and R. Mezzenga, *ACS Nano*, 2018, **12**, 5141–5148.
- M. Arcari, E. Zuccarella, R. Axelrod, J. Adamcik, A. Sánchez-Ferrer, R. Mezzenga and G. Nyström, *Biomacromolecules*, 2019, **20**, 1288–1296.
- S. Elazzouzi-Hafraoui, Y. Nishiyama, J.-L. Putaux, L. Heux, F. Dubreuil and C. Rochas, *Biomacromolecules*, 2008, **9**, 57–65.
- J. Hanley, L. Godbout and D. G. Gray, *Cellulose*, 1997, **4**, 209–220.
- J. Majoinen, J. Hassinen, J. S. Haataja, H. T. Rekola, E. Kontturi, M. A. Kostianinen, R. H. A. Ras, P. Törmä and O. Ikkala, *Adv. Mater.*, 2016, **28**, 5262–5267.
- K. Conley, L. Godbout, M. A. (Tony) Whitehead and T. G. M. van de Ven, *Carbohydrate Polymers*, 2016, **135**, 285–299.
- K. M. Conley, L. Godbout, M. A. Whitehead and T. G. M. van de Ven, *Cellulose*, 2017, **24**, 5455–5462.
- Y. Ogawa, *Nanoscale*, DOI:10.1039/C9NR06044H.
- C. Schütz, M. Agthe, A. B. Fall, K. Gordeyeva, V. Guccini, M. Salajková, T. S. Plivelic, J. P. F. Lagerwall, G. Salazar-Alvarez and L. Bergström, *Langmuir*, 2015, **31**, 6507–6513.
- J. Araki and S. Kuga, *Langmuir*, 2001, **17**, 4493–4496.
- E. Jin, J. Guo, F. Yang, Y. Zhu, J. Song, Y. Jin and O. J. Rojas, *Carbohydr Polym*, 2016, **143**, 327–335.
- J. Gong, J. Li, J. Xu, Z. Xiang and L. Mo, *RSC Adv.*, 2017, **7**, 33486–33493.
- G. Sèbe, F. Ham-Pichavant, E. Ibarboure, A. L. C. Koffi and P. Tingaut, *Biomacromolecules*, 2012, **13**, 570–578.
- J. Gong, L. Mo and J. Li, *Carbohydr Polym*, 2018, **195**, 18–28.
- Y. Kuang, X. Li, P. Luan, X. Zhang, J. Xu, L. Mo, J. Gong and J. Li, *Cellulose*, 2020, **27**, 3167–3179.
- X. Li, J. Li, J. Gong, Y. Kuang, L. Mo and T. Song, *Carbohydr Polym*, 2018, **183**, 303–310.

- 32 W. P. Flauzino Neto, J.-L. Putaux, M. Mariano, Y. Ogawa, H. Otaguro, D. Pasquini and A. Dufresne, *RSC Adv.*, 2016, **6**, 76017–76027.
- 33 Q. Wu, J. Xu, Z. Wu, S. Zhu, Y. Gao and C. Shi, *Carbohydrate Polymers*, 2020, **235**, 115962.
- 34 J. M. González-Domínguez, A. Ansón-Casaos, L. Grasa, L. Abenia, A. Salvador, E. Colom, J. E. Mesonero, J. E. García-Bordejé, A. M. Benito and W. K. Maser, *Biomacromolecules*, 2019, **20**, 3147–3160.
- 35 Y. Yue, C. Zhou, A. D. French, G. Xia, G. Han, Q. Wang and Q. Wu, *Cellulose*, 2012, **19**, 1173–1187.
- 36 Z. Ling, X. Zhang, G. Yang, K. Takabe and F. Xu, *Industrial Crops and Products*, 2018, **112**, 541–549.
- 37 A. G. de Souza, M. T. Junqueira, G. F. de Lima, V. K. Rangari and D. S. Rosa, *J Polym Environ*, 2020, **28**, 1150–1159.
- 38 L. Xing, J. Gu, W. Zhang, D. Tu and C. Hu, *Carbohydrate Polymers*, 2018, **192**, 184–192.
- 39 M. Hasani, E. D. Cranston, G. Westman and D. G. Gray, *Soft Matter*, 2008, **4**, 2238–2244.
- 40 B. J. C. Duchemin, *Green Chem.*, 2015, **17**, 3941–3947.
- 41 J. Bouchard, M. Méthot, C. Fraschini and S. Beck, *Cellulose*, 2016, **23**, 3555–3567.
- 42 A. D. French, *Cellulose*, 2014, **21**, 885–896.
- 43 D. L. Morgado and E. Frollini, 2011, **21**, 7.
- 44 B. A. P. Ass, M. N. Belgacem and E. Frollini, *Carbohydrate Polymers*, 2006, **63**, 19–29.
- 45 P. Pavlov and V. Makazchieva, *Fibre Chem*, 1993, **24**, 285–286.
- 46 E. J. Foster, R. J. Moon, U. P. Agarwal, M. J. Bortner, J. Bras, S. Camarero-Espinosa, K. J. Chan, M. J. D. Clift, E. D. Cranston, S. J. Eichhorn, D. M. Fox, W. Y. Hamad, L. Heux, B. Jean, M. Korey, W. Nieh, K. J. Ong, M. S. Reid, S. Rennecker, R. Roberts, J. A. Shatkin, J. Simonsen, K. Stinson-Bagby, N. Wanasekara and J. Youngblood, *Chem. Soc. Rev.*, 2018, **47**, 2609–2679.
- 47 R. R. Lahiji, X. Xu, R. Reifengerger, A. Raman, A. Rudie and R. J. Moon, *Langmuir*, 2010, **26**, 4480–4488.
- 48 O. M. Vanderfleet, M. S. Reid, J. Bras, L. Heux, J. Godoy-Vargas, M. K. R. Panga and E. D. Cranston, *Cellulose*, 2019, **26**, 507–528.
- 49 M. Labet and W. Thielemans, *Cellulose*, 2011, **18**, 607–617.
- 50 B. Risteen, G. Delepierre, M. Srinivasarao, C. Weder, P. Russo, E. Reichmanis and J. Zoppe, *Small*, 2018, **14**, 1802060.
- 51 S. Wohlhauser, G. Delepierre, M. Labet, G. Morandi, W. Thielemans, C. Weder and J. O. Zoppe, *Macromolecules*, 2018, **51**, 6157–6189.
- 52 J. O. Zoppe, A. V. M. Dupire, T. G. G. Lachat, P. Lemal, L. Rodriguez-Lorenzo, A. Petri-Fink, C. Weder and H.-A. Klok, *ACS Macro Lett.*, 2017, **6**, 892–897.
- 53 K. Heise, G. Delepierre, A. King, M. Kostianen, J. Zoppe, C. Weder and E. Kontturi, *Angewandte Chemie International Edition*, DOI:10.1002/anie.202002433.
- 54 S. Beck, M. Méthot and J. Bouchard, *Cellulose*, 2015, **22**, 101–116.
- 55 T. Abitbol, D. Kam, Y. Levi-Kalishman, D. G. Gray and O. Shoseyov, *Langmuir*, 2018, **34**, 3925–3933.
- 56 N. Lin and A. Dufresne, *Nanoscale*, 2014, **6**, 5384–5393.
- 57 A. Potthast, J. Röhrling, T. Rosenau, A. Borgards, H. Sixta and P. Kosma, *Biomacromolecules*, 2003, **4**, 743–749.
- 58 R. J. Maurer, A. F. Sax and V. Ribitsch, *Cellulose*, 2013, **20**, 25–42.
- 59 S. Shafiei-Sabet, W. Y. Hamad and S. G. Hatzikiriakos, *Langmuir*, 2012, **28**, 17124–17133.
- 60 Y. Xu, A. Atrens and J. R. Stokes, *Advances in Colloid and Interface Science*, 2020, **275**, 102076.
- 61 J. D. Kittle, X. Du, F. Jiang, C. Qian, T. Heinze, M. Roman and A. R. Esker, *Biomacromolecules*, 2011, **12**, 2881–2887.
- 62 M. Xu, K. D. M. Harris and J. M. Thomas, *J. Am. Chem. Soc.*, 2008, **130**, 5880–5882.
- 63 D. M. Lyons, J. P. McGrath and M. A. Morris, *J. Phys. Chem. B*, 2003, **107**, 4607–4617.
- 64 H. S. Kim, Y. Nishiyama, K. Ideta, J. Miyawaki, Y. Matsushita, J. I. Park, I. Mochida and S. H. Yoon, *Journal of Industrial and Engineering Chemistry*, 2013, **19**, 1673–1679.
- 65 S. Soares, N. M. P. S. Ricardo, S. Jones and F. Heatley, *European Polymer Journal*, 2001, **37**, 737–745.
- 66 X. Guo, Y. Wu and X. Xie, *Sci Rep*, 2017, **7**, 14207.
- 67 C. Aulin, S. Ahola, P. Josefsson, T. Nishino, Y. Hirose, M. Österberg and L. Wågberg, *Langmuir*, 2009, **25**, 7675–7685.
- 68 I. Usov, G. Nyström, J. Adamcik, S. Handschin, C. Schütz, A. Fall, L. Bergström and R. Mezzenga, *Nat Commun*, 2015, **6**, 7564.
- 69 S. Allenmark, *Chirality*, 2003, **15**, 409–422.
- 70 T. Uto, S. Mawatari and T. Yui, *J. Phys. Chem. B*, 2014, **118**, 9313–9321.
- 71 L. Onsager, *Annals of the New York Academy of Sciences*, 1949, **51**, 627–659.
- 72 H. H. Wensink and G. J. Vroege, *J. Chem. Phys.*, 2003, **119**, 6868–6882.
- 73 W. Chen and D. G. Gray, *Langmuir*, 2002, **18**, 633–637.
- 74 X. M. Dong, T. Kimura, J.-F. Revol and D. G. Gray, *Langmuir*, 1996, **12**, 2076–2082.
- 75 D. G. Gray and X. Mu, *ACS Omega*, 2016, **1**, 212–219.
- 76 S. Tomar, M. M. Green and L. A. Day, *J. Am. Chem. Soc.*, 2007, **129**, 3367–3375.
- 77 Z. Dogic and S. Fraden, *Langmuir*, 2000, **16**, 7820–7824.
- 78 P. J. Collings and M. Hird, *Introduction to Liquid Crystals: Chemistry and Physics*, CRC Press, 2017.
- 79 J. Van Rie, C. Schütz, A. Gençer, S. Lombardo, U. Gasser, S. Kumar, G. Salazar-Alvarez, K. Kang and W. Thielemans, *Langmuir*, 2019, **35**, 2289–2302.
- 80 P. Saha and V. A. Davis, *ACS Appl. Nano Mater.*, 2018, **1**, 2175–2183.
- 81 S. Beck and J. Bouchard, *Nordic Pulp & Paper Research Journal*, 2014, **29**, 6–14.
- 82 C. Li, J. Evans, N. Wang, T. Guo and S. He, *Sci Rep*, 2019, **9**, 11290.
- 83 C. Honorato-Rios, A. Kuhnhold, J. R. Bruckner, R. Dannert, T. Schilling and J. P. F. Lagerwall, *Front. Mater.*, DOI:10.3389/fmats.2016.00021.
- 84 B. Frka-Petesic, B. Jean and L. Heux, *EPL*, 2014, **107**, 28006.
- 85 K. J. De France, K. G. Yager, T. Hoare and E. D. Cranston, *Langmuir*, 2016, **32**, 7564–7571.
- 86 F. Smalenburg, H. R. Vutukuri, A. Imhof, A. van Blaaderen and M. Dijkstra, *J Phys Condens Matter*, 2012, **24**, 464113.
- 87 M. Houssa, L. F. Rull and S. C. McGrother, *J. Chem. Phys.*, 1998, **109**, 9529–9542.
- 88 D. Frenkel, *Nature Mater*, 2015, **14**, 9–12.
- 89 R. F. Nickerson and J. A. Habrle, *Ind. Eng. Chem.*, 1947, **39**, 1507–1512.
- 90 M. S. Reid, M. Villalobos and E. D. Cranston, *Langmuir*, 2017, **33**, 1583–1598.
- 91 E. Niinivaara, M. Faustini, T. Tammelin and E. Kontturi, *Langmuir*, 2015, **31**, 12170–12176.
- 92 V. S. J. Craig and M. Plunkett, *Journal of Colloid and Interface Science*, 2003, **262**, 126–129.
- 93 J. Schindelin, *Fiji: an open-source platform for biological-image analysis*, 2012, vol. 9(7).



The self-assembly behavior of CNCs from cellulose II is different than cellulose I, despite having similar shape, surface charge density and a right-handed twist. Longer pitch chiral nematic liquid crystals formed but over much longer time periods.